J Mater Sci (2016) 51:3329–3336
DOI 10.1007/s10853-015-9648-y

Preparation of (001) preferentially oriented titanium thin films by ion-beam sputtering deposition on thermal silicon dioxide

Imrich Gablech[1,2] · Vojtěch Svatoš[1,2] · Ondřej Caha[3,4] · Miloš Hrabovský[1,5] · Jan Prášek[1,2] · Jaromír Hubálek[1,2] · Tomáš Šikola[1,5]

Received: 6 August 2015 / Accepted: 6 December 2015 / Published online: 21 December 2015

Abstract We propose the ion-beam sputtering deposition providing Ti thin films of desired crystallographic orientation and smooth surface morphology not obtainable with conventional deposition techniques such as magnetron sputtering and vacuum evaporation. The sputtering was provided by argon broad ion beams generated by a Kaufman ion-beam source. In order to achieve the optimal properties of thin film, we investigated the Ti thin films deposited on an amorphous thermal silicon dioxide using X-ray diffraction, and atomic force microscopy. We have optimized deposition conditions for growing of thin films with the only (001) preferential orientation of film crystallites, and achieved ultra-low surface roughness of 0.55 nm. The deposited films have been found to be stable upon annealing up to 300 °C which is often essential for envisaging subsequent deposition of piezoelectric AlN thin films.

✉ Imrich Gablech
imrich.gablech@ceitec.vutbr.cz

[1] Central European Institute of Technology, Brno University of Technology, Technická 3058/10, 61600 Brno, Czech Republic

[2] Department of Microelectronics, Faculty of Electrical Engineering and Communication, Brno University of Technology, Technická 3058/10, 61600 Brno, Czech Republic

[3] Central European Institute of Technology, Masaryk University, Kamenice 753/5, 62500 Brno, Czech Republic

[4] Department of Condensed Matter Physics, Faculty of Science, Masaryk University, Kotlářská 2, 60200 Brno, Czech Republic

[5] Institute of Physical Engineering, Brno University of Technology, Technická 2896/2, 61669 Brno, Czech Republic

Introduction

Titanium has been a frequently used material in microelectronics and MEMS technology. Titanium thin films have been used as sensing electrodes, buffer, or adhesive layers. The advantages of titanium thin films are good electric conductivity, extraordinary chemical resistivity, thermal stability, high hardness, high melting point, and lower number of crystallographic imperfections [1–5]. Crystallographic orientation of titanium thin films has to be controlled during the deposition process to obtain specific properties (e.g., mechanical, chemical) suitable for an eventually required application [6, 7]. Some of recent MEMS devices use the piezoelectric effect for energy harvesting or sensing purposes [8]. Titanium has been often utilized in MEMS technology as a compatible material for fabrication of thin conductive underlying electrodes on which the piezoelectric layers are deposited [6].

The crystallographic orientation of titanium thin films is crucial for properties of consequently deposited piezoelectric layers [9]. Obviously, the properties of these layers (AlN, ZnO), namely electromechanical properties, are significantly affected by the crystallographic orientation, surface morphology, and the roughness layers beneath [10]. There have been many papers published investigating the degree of orientation which is strongly dependent on the texture and roughness of underlying material [11, 12]. Titanium thin films have been usually deposited by the physical vapor deposition (PVD) particularly magnetron sputtering [13] or e-beam evaporation [4]. Obviously, different deposition parameters result in various film properties. Considering the surface roughness, low process pressure during deposition (i.e., $<5 \times 10^{-3}$ mbar) usually results in a smooth film surface (i.e., R_{rms} <10 nm). At higher deposition pressure (i.e., $<14 \times 10^{-3}$ mbar), the

titanium RMS surface roughness of 45 nm was achieved. Consequently, a negative effect on the piezoelectric coefficients of AlN layers deposited on Ti thin film due to a porous surface was observed [10]. The magnetron sputtering is the most frequent method for titanium thin films deposition [14]. Titanium thin films deposited by the magnetron sputtering generally possess (100), (001), and (101) crystallographic orientations of crystallites parallel to the surface [1]. Without a special modification of the magnetron sputtering process (closed-field unbalanced magnetron sputtering, pulsed magnetron sputtering), the number of various and independent deposition parameters capable of optimizing deposited layers is limited [15, 16]. Due to the lack of the process control parameters, it is often an issue to achieve thin films of desired properties for specific application.

In this paper, we report on a deposition of Ti thin film with the (001) preferential crystallite orientation growth on amorphous thermal silicon dioxide using a 3-grid radio frequency inductive-coupled plasma (RFICP) Kaufman ion-beam source. As generally known, the Kaufman ion-beam source provides more efficient control and optimization of the deposition process compared to the conventional deposition method [17, 18]. Here, ion-beam flux, energy, and ion-beam geometry, can be controlled independently. We have studied the influence of deposition parameters on properties of Ti thin films especially on their preferential crystallographic orientation and topography.

Experimental details

Deposition process

The deposition of titanium layers was done on substrates (20 × 20) mm diced from 4-inch P-type silicon wafer with the (100) crystallographic orientation and the resistivity of 6–12 Ω cm covered with thermal silicon dioxide (ON Semiconductor). The thickness of silicon dioxide was approximately 1 μm. Before the sputtering process, we cleaned all substrates in the standard piranha solution (96 % H_2SO_4 + 30 % H_2O_2 in the 3:1 ratio) for 5 min, rinsed in deionized water (18.7 MΩ cm), and dried them by compressed nitrogen.

The deposition process was done using the ion-beam sputtering apparatus (Bestec) equipped with RFICP Kaufman ion-beam source (Kaufman & Robinson—KRI®) with the molybdenum 3-grid dished focused ion optics (4 cm in diameter and with 45° ellipse pattern) providing an Ar ion beam bombarding the Ti target under an incidence angle of 45°. The 99.9996 % pure argon gas was used during the deposition process. Titanium of 99.995 % purity (Porexi) was sputtered from a (100 × 100) mm target. Reduction of the ion-beam space charge was provided by KRI LFN 2000 charge neutralizer (KRI®). Before each deposition process, the sputtering chamber was evacuated to pressure of 5×10^{-9} mbar using a turbomolecular HiPace 1200 turbopump (Pfeiffer Vacuum) with the pumping speed of 1200 l/s for argon backed by TriScroll® 300 series dry scroll vacuum pump (Agilent Technologies). The schematic illustration of the apparatus setup including all significant dimensions and angles is shown in Fig. 1.

The operation parameters of the deposition process are beam voltage (BV) determining energy of the ion beam at the target, acceleration voltage (AV) controlling the extraction and the optical parameters of the beam, beam current (BC) equal to the ion-beam current at the target, radio frequency power (RFP) supplied to the discharge, argon flow rate, and substrate temperature. During all deposition experiments, the substrate was rotating with the speed of 5 rpm. A particular setup of the major parameters for individual deposition experiments is listed in Tables 1 and 2. In all deposition experiments, the substrate was not heated up and its temperature was affected only by the energy of sputtered material. The substrate temperature did not exceed the value of 100 °C. The Inficon SQM-242 card with a quartz crystal sensor was used to monitor the deposition parameters as thickness and rate of deposition.

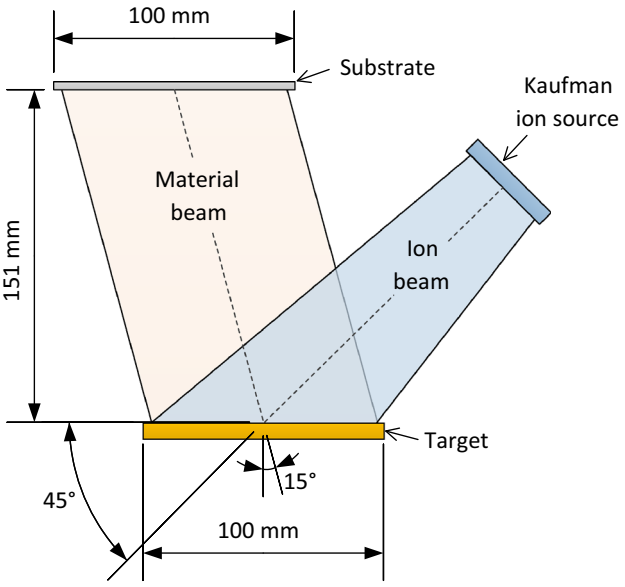

Fig. 1 Schematic of sputtering apparatus geometry with Kaufman ion-beam source

Table 1 Ion-beam source experimental setup (BV, AV, BC, RFP, Ar flow) and deposition pressure and rate

Sample no.	BV (V)	AV (V)	BC (mA)	RFP (W)	Ar flow (sccm)	Process pressure (mbar)	Deposition rate (Å/s)
1–1	200	−100	6.0	74	2.2	2.1×10^{-4}	0.04–0.06
1–2	400	−80	13.0	73	2.4	2.2×10^{-4}	0.15–0.18
1–3	500	−100	18.0	86	2.6	2.3×10^{-4}	0.24–0.26
1–4	600	−120	23.0	94	2.8	2.4×10^{-4}	0.32–0.34
1–5	700	−140	29.0	107	3.0	2.5×10^{-4}	0.42–0.44
1–6	800	−160	36.0	118	3.3	2.6×10^{-4}	0.56–0.58
1–7	900	−180	43.0	130	3.6	2.7×10^{-4}	0.70–0.72
1–8	1000	−200	50.0	140	3.9	2.9×10^{-4}	0.84–0.86
1–9	1200	−240	65.0	168	4.4	3.1×10^{-4}	1.18–1.20
1–10	1200	−600	82.0	188	5.3	3.5×10^{-4}	1.49–1.51

Table 2 Ion-beam source setup deposition pressure and rate in experiments on optimization of the film structure with respect to the (001) preferential crystallographic orientation

Sample no.	BV (V)	AV (V)	BC (mA)	RFP (W)	Ar flow (sccm)	Deposition pressure (mbar)	Deposition rate (Å/s)
2–1	200	−100	6.0	73	2.1	1.9×10^{-4}	0.04–0.06
2–2	200	−120	6.0	74	2.1	1.9×10^{-4}	0.04–0.07
2–3	200	−140	7.0	73	2.1	1.9×10^{-4}	0.05–0.07
2–4	200	−160	7.0	74	2.1	1.9×10^{-4}	0.05–0.07
2–5	200	−180	8.0	74	2.2	2.0×10^{-4}	0.06–0.07
2–6	200	−200	8.0	73	2.2	2.0×10^{-4}	0.07–0.08
2–7	200	−220	9.0	74	2.2	2.0×10^{-4}	0.07–0.09
2–8	200	−240	9.0	74	2.2	2.0×10^{-4}	0.07–0.09

Diagnostic methods

X-ray diffraction (XRD) technique was used for crystallography analysis. These analysis were done with X-ray diffractometer (SmartLab, Rigaku) containing a linear D/teX Ultra detector and working in the Bragg–Brentano (BB) focusing geometry. Pole figures were measured using parallel beam setup with multilayer parabolic mirror as a collimator and a scintillation detector. The surface roughness (R_{RMS}) of deposited layers was investigated by Atomic Force Microscopy (AFM, Dimension Icon, Bruker) in the ScanAsyst®-Air mode using the corresponding probe (ScanAsyst-Air) with the cantilever spring constant of 0.4 N m^{-1} and tip radius of 2 nm.

Annealing procedure

The deposited samples were exposed to an annealing procedure using the annealing oven (Vakuum Praha). The annealing procedure was done for three temperatures 100, 200, and 300 °C at the pressure of 5×10^{-7} mbar. The annealing protocol was set with following parameters: heating rate 5 °C per minute; peak temperature was held for 60 min; cooling rate 5 °C per minute.

Results and discussion

In the first series of experiments, we set the absolute values of BV and AV in the ratio 5:1 to reduce the flux of electrons according to the rule of electron-backstreaming limit experimentally determined by the manufacturer [19]. The higher ratios of BV and AV cause flowing of electrons (secondary electrons, neutralizing electrons) through ion optics into the ion source affecting the discharge. Utilizing the feedback control, we set BC appropriately to BV and AV according to a recommendation in the KRI® datasheet. These values of the ion-beam current were optimum ones at which a direct impingement of beam ions into the accelerator and decelerator grids were suppressed.

The first sample (Sample 1–1) was deposited using higher AV because it was not possible to keep stable plasma discharge, and the last one (Sample 1–10) was deposited at maximum possible voltage settings of ion-beam source. In Table 1, different settings of deposition parameters together with the resultant deposition pressure and deposition rate are listed.

We used XRD in the BB setup with the 2θ angle ranging from 20° to 90° to perform the phase analysis of all deposited layers. We detected diffraction peaks belonging to (100), (101), and (001) crystallographic planes. For

(001) crystallographic plane, second-order diffraction 002 was measured since the first-order diffraction is forbidden. However, in the following text we will note it as (001). The corresponding X-ray diffractogram is depicted in Fig. 2. The diffractograms show also the slight peak at 2θ of 68° to 70° which originates from the silicon substrate and sometimes a very weak peak corresponding to the fourth-order diffraction on the Ti (001) plane at 83°. The obtained results show that crystallographic orientation of sputtered layer depends mainly on ion energy which is given by BV. In case of low ion-beam energies (200 eV and 400 eV, samples 1–1 and 1–2, respectively), the required (001) preferential crystallographic orientation of the crystallites with a small contribution of (100) planes parallel to the surface was obtained. On the other hand, the (100) plane orientation was much more represented at higher ion-beam energies, namely in the range of BV from 500 to 1000 V (Samples 1–3 to 1–8). At the highest ion-beam energy (BV of 1200 V, sample 1–9 and 1–10), the (101) plane orientation was observed along with the (001) and (100) ones.

The second series of experiments was aimed at finding the optimal deposition conditions in order to achieve the only (001) preferential orientation of crystallites in the Ti films parallel to the surface. We were changing AV (affecting ion extraction and ion-beam formation, and thus the ion-beam space charge as well) from −100 to −240 V at the fixed BV of 200 V (i.e., at the constant ion-beam energy of 200 eV). All deposition parameters are summarized in Table 2. The obtained X-ray diffractograms for all prepared samples are shown in Fig. 3.

As can be seen in Fig. 3, at an AV value of −220 V (sample 2–7), it is clear that the preferential (001) orientation of thin film was achieved. The other settings of the AV resulted in a minor peak in the diffractogram proving the presence of (100) plane. This behavior was probably attributed to distinct values of space charge potential depending on the AV setting, and providing different energies of charge-exchange argon ions which are leaving the beam and bombarding the substrate surface [17]. In this way, these factors can assist in the growths of thin films and modify their properties similarly to ion-beam-assisted techniques [20]. These results of performed optimizations showed the possibility of producing the titanium layer with only one preferential (001) plane orientation. We have determined the lattice parameters of the optimized thin films; the c lattice parameter was ascertained $c = 4.72$ Å while the lattice parameter was determined by grazing incidence diffraction $a = 2.95$ Å. The tabulated values of these parameters are $a = 2.951$ Å and $c = 4.695$ Å [21].

Carrying out identical experiments for four times, we proved a good repeatability of the results. In all four cases, we obtained the identical diffractograms of thin films prepared in the independent experiments with the same deposition parameters leading to the (001) preferential orientation as sample 2–7.

Full width at half maximum (FWHM) of the diffraction peak belonging to (001) planes was 0.4° for all samples with good reproducibility. This width corresponds to the average coherently diffracting domain of 22 nm calculated using Scherrer formula [22]. This value is underestimating the real average crystallite size since the internal strain is neglected. The higher order diffractions were too weak to be detected with sufficient statistics and further analysis was not possible.

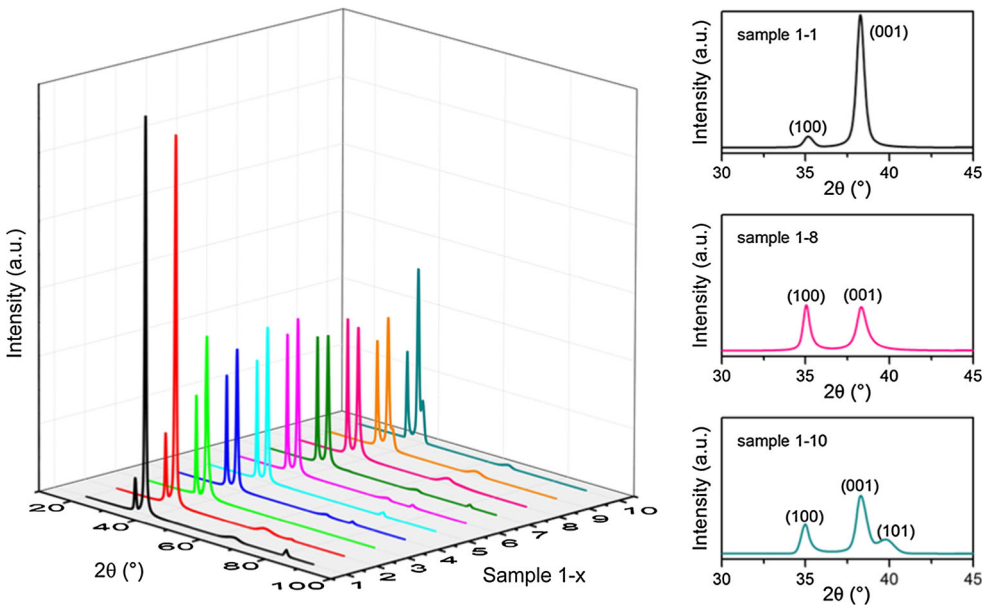

Fig. 2 X-ray diffractograms of deposited thin films obtained with different BV and AV; 3D plot of diffractograms of all samples prepared at deposition parameters listed in Table 1 (*left*), three detailed diffractograms showing the samples with the most distinguished crystallographic orientations of the films (*right*)

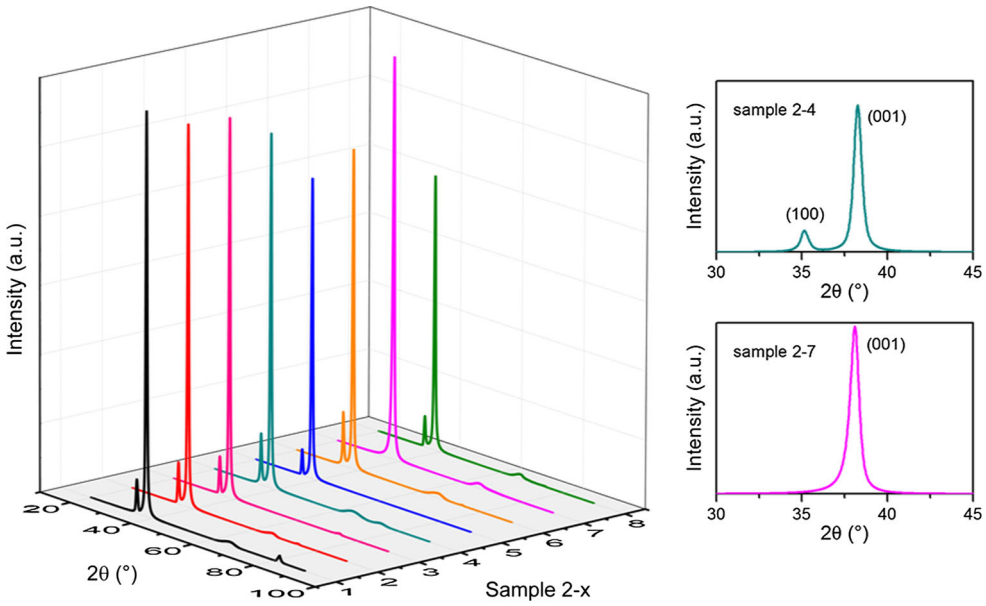

Fig. 3 X-ray diffractograms of thin films deposited at the fixed BV of 200 V and different AVs; 3D plot of diffractograms of all samples prepared at deposition parameters listed in Table 2 (*left*), two detailed diffractograms showing the samples with most presented (100) crystallographic orientation (sample 2–4) and the layer with only (001) orientation (sample 2–7) (*right*)

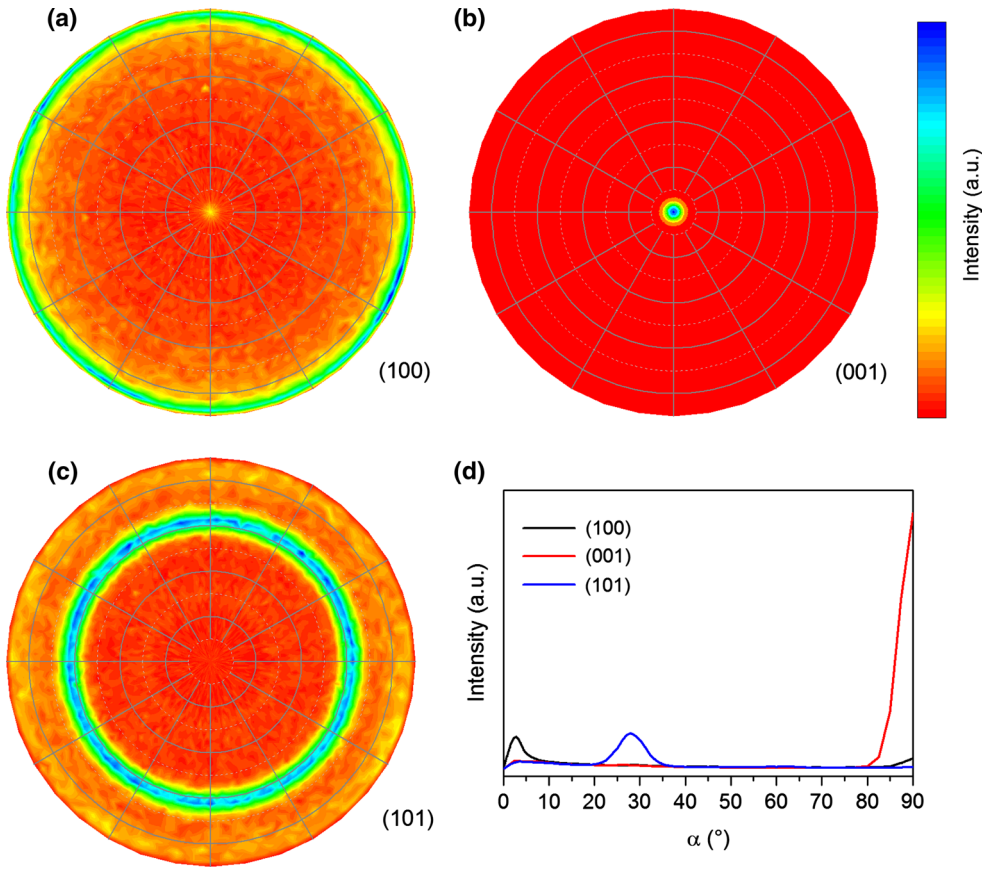

Fig. 4 Pole figures of the sample 2–7 with the optimized preferential orientation; **a** (100) plane angular (i.e., polar and azimuthal) distribution, **b** (001) plane angular distribution, **c** (101) plane angular distribution **d** azimuthally averaged intensity profiles extracted from the preceding pole figures plotted as a function of the crystallographic plane inclination with respect to the sample normal

Further, we performed the pole figure analysis of the optimized sample (i.e., the sample 2–7) for the diffraction angles belonging to (100), (001), and (101) diffraction planes to determine their preferential orientation. The pole figures shown in Fig. 4 are the stereographic projections of the diffracted intensity plotted with respect to the sample coordinates, i.e., pole figure center corresponds to the crystallographic planes parallel to the surface while the edge of the circle corresponds to the planes being perpendicular to the surface. In the previously shown Bragg–

Brentano scans, one can detect only crystallographic planes parallel to the surface. The experimental results show the (001) planes are predominantly oriented parallel to the sample surface, while (100) planes are predominantly perpendicular to the surface. The average misorientation of individual crystallites determined from FWHM of the pole figure peak is 5° (see Fig. 4b, d). Accordingly, the (100) planes being perpendicular to (001) planes reveal their maximum intensity at the edge of the pole figure as shown in Fig. 4a, d. The weak maximum at the pole figure center in Fig. 4a is caused by the fact that the diffraction peaks belonging to (100) and (001) planes are partially overlapping in the angle 2θ and they are not completely separated with used experimental resolution (see Fig. 4d). The angle between the (101) and (001) crystallographic planes in the Ti lattice is 61.3° which perfectly corresponds to the

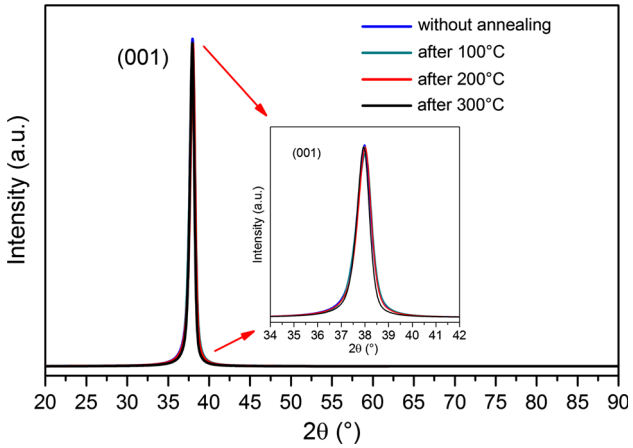

Fig. 5 X-ray diffractograms obtained after each annealing step up to 300 °C for 1 h

Table 3 Measured R_{RMS} surface roughness of samples prepared with different BV and AV settings

Sample no.	BV (V)	AV (V)	R_{RMS} (nm)
1–1	200	−100	0.72 ± 0.08
2–7	200	−220	0.55 ± 0.07
1–2	400	−80	0.73 ± 0.09
1–4	600	−120	0.76 ± 0.09
1–6	800	−160	0.76 ± 0.12
1–8	1000	−200	0.75 ± 0.09
1–9	1200	−240	0.66 ± 0.08
1–10	1200	−600	0.67 ± 0.08

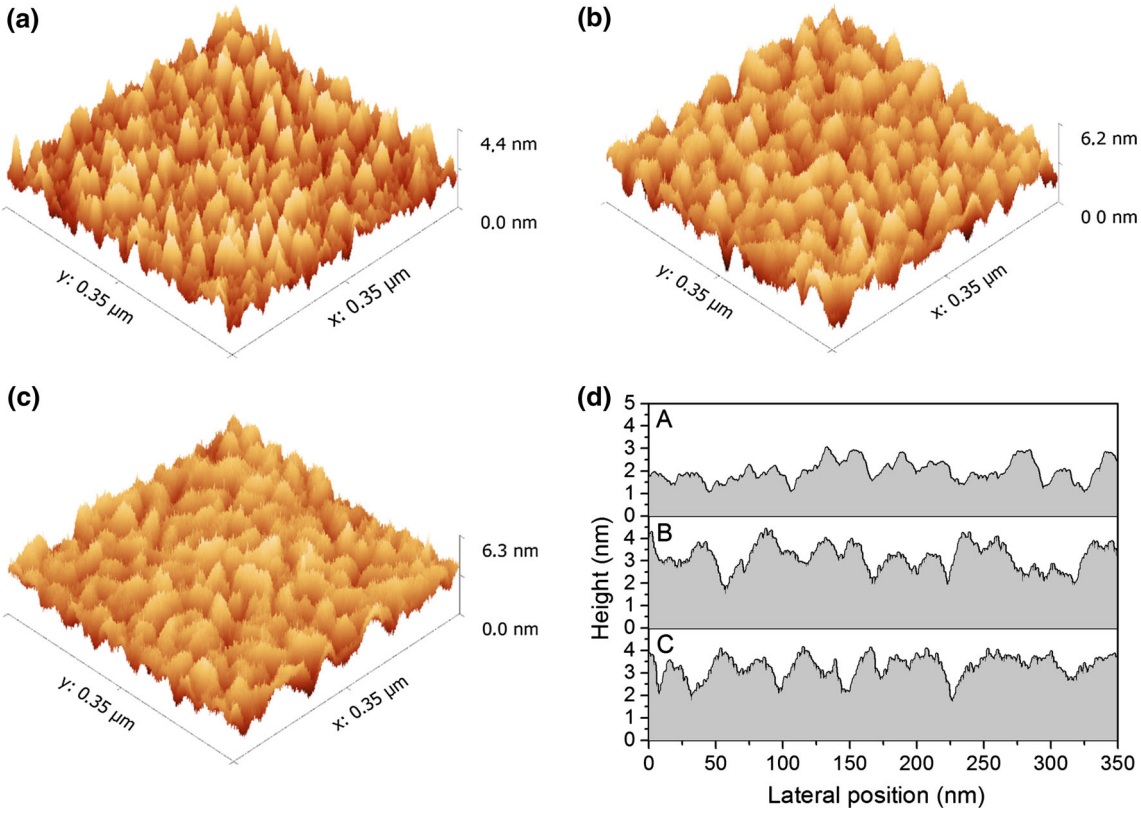

Fig. 6 Surface topography obtained by AFM; **a** the sample 2–7 with the (001) preferential crystallographic orientation; **b** the sample 1–8 with the (100) and (001) crystallographic orientations; **c** the sample 1–10 with (100), (001), and (101) crystallographic planes; **d** profiles corresponding to the three shown AFM surface topography

observed maximum in the pole Fig. 4c. All the three pole figures have a perfect rotational symmetry which means the orientation of the individual crystallites in the azimuthal direction is random with no indication of any preferred azimuthal direction. However, we expected such behavior since the substrate was rotating during the Ti deposition and therefore no unique azimuthal axis is present.

Consequent deposition of some layers such as AlN or ZnO over a titanium film often requires process temperatures up to 300 °C [8]. Considering this fact, we exposed several samples (sample 2–7) with the optimized (001) preferential crystallites orientation to an annealing process in vacuum of 5×10^{-7} mbar. The annealing process was supposed to simulate conditions similar to those needed for deposition of these binary thin film compounds on a titanium layer and thus to learn its possible thermal instability. The consequent XRD analysis (see Fig. 5) shows no obvious changes in the crystal lattice after three different annealing processes which were carried out for three maximum temperatures 100, 200, and 300 °C.

We used the AFM in the ScanAsyst® mode to determine the surface topography and roughness of deposited thin films. Figure 6a shows topography of the sample 2–7 containing titanium crystallites with the preferential orientation (001) with surface roughness of only 0.55 nm. Topography of the sample 1–8 containing crystallites with both (100) and (001) crystallographic planes (see Fig. 2) parallel to the surface is shown in Fig. 6b. This sample has one of the highest surface roughnesses with a value of 0.75 nm. We attribute this fact to the equal distribution of these two crystallographic orientations recognizable as sharp peaks (001) combined with the rounded elongated islands (100). Figure 6c shows the topography of the sample 1–10 where the major contribution to the crystallographic structure comes from the crystallographic orientation 001 along with (100) and (101) planes. We presume this fact is reflected in a surface roughness of the value 0.67 nm which is lower compared to the previous sample. The individual AFM profiles of these three samples (sample 2–7, 1–8, 1–10) are depicted in Fig. 6d.

The results of the AFM measurement are listed in Table 3. The table contains the values of RMS surface roughness including its standard deviations for each sample with corresponding BV and AV. It is obvious that the sample 2–7 possessing the (001) preferential orientation has the lowest surface roughness.

Conclusion

We have presented the optimized deposition process of the (001) preferentially oriented titanium thin film using the Kaufman ion-beam source. The performed experiments have shown that both the low energy and the low ion-beam current are necessary for deposition of highly oriented Ti thin films with the only (001) preferential orientation of films crystallites parallel to the surface.

The crystallites with the (100) orientation parallel to the surface were present in the thin films deposited at higher ion-beam energies (BV of 400 V and higher), and those with the (101) plane parallel to the surface in the films deposited at the highest value of ion-beam energy (BV of 1200 V). The R_{RMS} roughness of all deposited films was less than 1 nm according to the AFM measurements which confirms an ultra-smooth character of surface. The lowest value of surface roughness is only 0.55 nm. We have shown that the surface roughness of thin films depends on the preferential crystallographic orientation.

The observed behavior and properties of the Ti thin films are attributed to specific deposition conditions provided by the Kaufman ion-beam source which generally are not achievable with the conventional magnetron sputtering.

Acknowledgement We acknowledge the support by the European Regional Development Fund (project No. CZ.1.05/1.1.00/02.0068). The work was also carried out with the support of the CEITEC Nano Core Facility under the CEITEC—open access project, ID number LM2011020, funded by the Ministry of Education, Youth and Sports of the Czech Republic under the activity "Projects of major infrastructures for research, development and innovations."

References

1. Chawla V, Jayaganthan R, Chawla AK, Chandra R (2009) Microstructural characterizations of magnetron sputtered Ti films on glass substrate. J Mater Process Technol 209(7):3444–3451. doi:10.1016/j.jmatprotec.2008.08.004
2. Chen C-N (2012) Fully quantitative characterization of CMOS–MEMS polysilicon/titanium thermopile infrared sensors. Sens Actuators B 161(1):892–900. doi:10.1016/j.snb.2011.11.058
3. Doll JC, Petzold BC, Ninan B, Mullapudi R, Pruitt BL (2010) Aluminum nitride on titanium for CMOS compatible piezoelectric transducers. J Micromech Microeng 20(2):25008. doi:10.1088/0960-1317/20/2/025008
4. López JM, Gordillo-Vázquez FJ, Fernández M, Albella JM (2001) Influence of oxygen on the morphological and structural properties of Ti thin films grown by ion beam-assisted deposition. Thin Solid Films 384(1):69–75. doi:10.1016/S0040-6090(00)01804-6
5. Tsuchiya T, Hirata M, Chiba N (2005) Young's modulus, fracture strain, and tensile strength of sputtered titanium thin films. Thin Solid Films 484(1–2):245–250. doi:10.1016/j.tsf.2005.02.024
6. Tran AT, Wunnicke O, Pandraud G, Nguyen MD, Schellevis H, Sarro PM (2013) Slender piezoelectric cantilevers of high quality

AlN layers sputtered on Ti thin film for MEMS actuators. Sens Actuators A 202:118–123. doi:10.1016/j.sna.2013.01.047
7. Jackson N, O'Keeffe R, Waldron F, O'Neill M, Mathewson A (2013) Influence of aluminum nitride crystal orientation on MEMS energy harvesting device performance. J Micromech Microeng. doi:10.1088/0960-1317/23/7/075014
8. Jackson N, Keeney L, Mathewson A (2013) Flexible-CMOS and biocompatible piezoelectric AlN material for MEMS applications. Smart Mater Struct. doi:10.1088/0964-1726/22/11/115033
9. Xiong J, Gu H-s HuK, M-z Hu (2010) Influence of substrate metals on the crystal growth of AlN films. Int J Miner Metall Mater 17(1):98–103. doi:10.1007/s12613-010-0117-y
10. Ababneh A, Alsumady M, Seidel H, Manzaneque T, Hernando-García J, Sánchez-Rojas JL, Bittner A, Schmid U (2012) c-axis orientation and piezoelectric coefficients of AlN thin films sputter-deposited on titanium bottom electrodes. Appl Surf Sci 259:59–65. doi:10.1016/j.apsusc.2012.06.086
11. Iriarte GF, Bjurstrom J, Westlinder J, Engelmark F, Katardjiev IV (2005) Synthesis of c-axis-oriented AlN thin films on high-conducting layers: Al, Mo, Ti, TiN, and Ni. IEEE Trans Ultrason Ferroelectr Freq Control 52(7):1170–1174. doi:10.1109/tuffc.2005.1504003
12. Boeshore SE, Parker ER, Lughi V, MacDonald NC, Bingert M (2005) Aluminum nitride thin films on titanium for piezoelectric microelectromechanical systems. In 2005 IEEE ultrasonics symposium, vol 1–4. New York, pp. 1641–1643
13. Jung MJ, Nam KH, Shaginyan LR, Han JG (2003) Deposition of Ti thin film using the magnetron sputtering method. Thin Solid Films 435(1–2):145–149. doi:10.1016/S0040-6090(03)00344-4
14. PalDey S, Deevi SC (2003) Single layer and multilayer wear resistant coatings of (Ti, Al)N: a review. Mater Sci Eng A 342(1–2):58–79. doi:10.1016/S0921-5093(02)00259-9
15. Jing FJ, Yin TL, Yukimura K, Sun H, Leng YX, Huang N (2012) Titanium film deposition by high-power impulse magnetron sputtering: influence of pulse duration. Vacuum 86(12):2114–2119. doi:10.1016/j.vacuum.2012.06.003
16. Henderson PS, Kelly PJ, Arnell RD, Bäcker H, Bradley JW (2003) Investigation into the properties of titanium based films deposited using pulsed magnetron sputtering. Surf Coat Technol 174–175:779–783. doi:10.1016/S0257-8972(03)00397-9
17. Harper JME, Cuomo JJ, Kaufman HR (1982) Technology and applications of broad-beam ion sources used in sputtering. 2. Applications. J Vac Sci Technol 21(3):737–756. doi:10.1116/1.571820
18. Kaufman HR, Cuomo JJ, Harper JME (1982) Technology and applications of broad-beam ion sources used in sputtering.1. Ion-source technology. J Vac Sci Technol 21(3):725–736. doi:10.1116/1.571819
19. Catalog The Kaufman & Robinson Inc. (2013) RFICP 40 ion optics supplement: molybdenum three-grid dished focused 4-cm diameter 45° ellipse
20. Sikola T, Spousta J, Dittrichova L, Nebojsa A, Perina V, Ceska R, Dub P (1996) Dual ion-beam deposition of metallic thin films. Surf Coat Technol 84(1–3):485–490. doi:10.1016/S0257-8972(95)02823-4
21. PDF-2 database entry 00-044-1294, ICDD-JCPDS
22. Patterson AL (1939) The scherrer formula for X-ray particle size determination. Phys Rev 56(10):978–982